



Natural Resources Conservation Service  
National Soil Survey Center  
Federal Building, Room 152  
100 Centennial Mall North  
Lincoln, NE 6850-8-3866

Phone: (402) 437-50-16  
FAX: (402) 437-5760

---

SUBJECT: SOI – Geophysical Assistance

May 24, 2014

TO: Ivan Dozier  
State Conservationist  
USDA-Natural Resources Conservation Service  
2118 West Park Court  
Champaign, IL 61821

File Code: 330-7

**Purpose:**

In this study, soil materials that have been excavated, replaced, and graded during surface-mining operations were assessed and mapped with electromagnetic induction (EMI) in Fulton County. Electromagnetic induction measures variations in apparent conductivity ( $EC_a$ ), which were associated with differences in clay and moisture contents; and variations in apparent magnetic susceptibility (IP, inphase response), which were associated with differences in management and the application of municipal sludge. In addition, the presence and distribution of joints in bedrock were studied in an area of Frankville soils with ground-penetrating radar (GPR) in Jo Daviess County. These cracks are common and have an impact on water and gas movement through the bedrock, and influence plant rooting depths and available soil moisture. The West Central Glaciated Soil Survey Region (SSR 10) and the Onalaska (WI) MLRA Soil Survey Offices provided GPR technical assistance for this study.

**Participants:**

Jim Doolittle, Research Soil Scientist, USDA-NRCS-NSSC, Newtown Square, PA  
Mike England, Soil Scientist, USDA-NRCS, Onalaska, WI  
Robert Nayden, Soil Conservation Technician, USDA-NRCS, Lewistown, IL  
Kim Smail, District Conservationist, USDA-NRCS, Lewistown, IL  
Roger Windhorn, Geologist, USDA-NRCS, Champaign, IL  
Dan Withers, Cartographic Technician, USDA-NRCS, Champaign, IL

**Activities:**

All activities were completed during the period of April 28 to May 1 2014.

**Summary:**

1. At both reclaimed surface mine spoil study sites in Fulton County, the average  $EC_a$  increased with increasing soil depths. The trend in  $EC_a$  is attributed principally to increasing moisture contents within increasing soil depths. The measured IP data appear to reflect differences in management practices among the individual fields surveyed. Higher or more anomalous IP responses in surface layers are attributed to differences in organic residue, surface moisture, soil compaction, and minerals (due to differences in fertilization, sludge applications, and management). Additional studies are warranted to better understand the role EMI can play in soil health.
2. In areas of Lenzburg soils, spatial  $EC_a$  patterns are complex and could not be associated with observed differences in soil drainage and landscape position.



3. To confirm some EMI interpretations, soil samples were collected at 24 sites. The concentrations of different metal in these samples were calculated by the New Jersey NRCS Soil Staff using a portable X-ray fluorescence (P-XRF) spectrometer. Our deepest appreciation is extended to Edwin Muniz and Richard Shaw for their assistance in this study.
4. In areas of regraded and cultivated Lenzburg soils at the Churchill Farm, based on the analysis of soil samples with P-XRF, the twelve most abundant metals present in the 0 to 60 cm soil layers were (in order of abundance): Fe, K, Ca, Ti, Mn, Zr, Ba, Co, Sr, Rb, Cr, and Zn.
5. As a result of the spatial IP patterns and knowledge of sludge applications to one field, the three fields studied at the Churchill Farm were grouped into two areas: fields 1 & 2 (combined), and field 3. With the exception of Ca and Co, the concentrations of all other analyzed metals were higher in the field that had received applications of sludge and displayed the most anomalous IP responses. Most notably, the concentration of Mn was 55% higher in the field that had received the municipal sludge.
6. The relationships between IP response and the concentration of metals within these two areas (Fields 1 & 2, and field 3) at the Churchill Farm were assessed using the Spearman rank correlation coefficient. Surprisingly, the correlations between IP response and the concentration of metals were generally higher in the fields that did not receive the sludge applications. This was not an expected result.
7. For the fields surveyed with EMI at the DoubleCluck Farm, linear spatial patterns appeared in both the  $EC_a$  and IP data sets. The spatial  $EC_a$  patterns cut directly across the landscape and are assumed to reflect differences in surface mining operations and reclamation processes. Compared with the spatial  $EC_a$  patterns, spatial IP patterns are more subdued. These more subdued spatial patterns followed the general directions in which the fields were surveyed [with EMI] and cultivated. These trends suggest that the use of traditional soil-landscape relationships to assess the variability in soil physiochemical properties may be inappropriate in areas of surface mined areas.
8. Results from a GPR detailed survey of joint patterns in an area of Frankville soil were disappointing. However, results from this study provided a greater understanding of how different soil properties influence GPR results and the clarity of interpretations.

It was the pleasure of Jim Doolittle and the National Soil Survey Center to be of assistance to your staff.

*/s/ Jonathan W. Hempel*

JONATHAN W. HEMPEL

Director

National Soil Survey Center

cc:

Ronald Collman, State Soil Scientist, USDA-NRCS, 2118 West Park Court, Champaign, IL 61821

Jim Doolittle, Research Soil Scientist, USDA-NRCS-NSSC, 11 Campus Blvd., Suite 200, Newtown Square, PA  
Mike England, Soil Scientist, USDA-NRCS, 1107 Riders Club Road, Onalaska, WI 54650-2079  
Paul Finnell, Soil Scientist/Soil Liaison SSR 11, USDA-NRCS-NSSC, MS 35, 100 Centennial Mall North, Lincoln, NE 68508-3866  
Edwin Muñiz, Assistant State Soil Scientist, USDA-NRCS, 220 Davidson Ave., 4th Floor, Somerset, NJ 08873-4115  
Travis Neely, Soil Survey Regional Director, SSR 11, USDA-NRCS, 6013 Lakeside Blvd., Indianapolis, Indiana 46278  
Caryl Radatz, Soil Survey Regional Director, SSR 10, USDA-NRCS, 375 Jackson Street, Suite 600, St. Paul, MN 55101-1854  
Michael Robotham, Acting National Leader, Soil Survey Research & Laboratory, USDA-NRCS-NSSC, MS 41, 100 Centennial Mall North, Lincoln, NE 68508-3866  
Kim Smail, District Conservationist, USDA-NRCS, Lewistown Service Center, 15381 N State 100 Highway, Lewistown, IL 61542-9456  
Richard Shaw, State Soil Scientist, USDA-NRCS, 220 Davidson Ave., 4th Floor, Somerset, NJ 08873-4115  
Robert Tegeler, MLRA Project Leader, USDA-NRCS, 2623 Sunrise Drive, Springfield, IL 62703  
Kevin Traastad, MLRA Project Leader, USDA-NRCS, 1107 Riders Club Road, Onalaska, WI 54650-2079  
Wes Tuttle, Soil Scientist, USDA-NRCS-NSSC, P.O. Box 60, 207 West Main Street, Room G-08, Federal Building, Wilkesboro, NC 28697  
Roger Windhorn, Geologist, USDA-NRCS, 2118 West Park Court, Champaign, IL 61821

**Technical Report on Geophysical Investigations conducted in Illinois  
on April 28 to May 1 2014**

**James A. Doolittle**

It is estimated that over 48,000 acres in Fulton County has been exposed to surface coal-mining operations (Spindler, 1981). According to Spindler (1981), most of this acreage consists of spoil composed of unconsolidated loess and till over rocky, shoveled-spoil materials. The spoil was created with bucket-wheel excavator and shovel combinations. The objectives of this study were to characterize spatial differences in soil properties and to improve interpretations for soil materials that have been excavated, replaced, and graded during surface mining operations. In this study, spatial variations in soil properties were inferred and mapped using electromagnetic induction (EMI). In addition, the concentration of heavy metals in samples extracted from twenty-four soil cores were analyzed using portable X-ray fluorescence (P-XRF).



Figure 1. These images show areas of Lenzburg soils that are being used as cropland and wildlife refuge. The field on the left has had its mine spoil overburden reshaped to the approximate pre-mined contours and restored to growing row crops according to topsoil and rooting medium depth requirements. The mine spoil area in the image on the right is used as a wildlife refuge and reflects practices that were permitted before the passage of the Illinois Surface-Mined Land Conservation and Reclamation Act of 1971.

**Equipment:**

An EM38-MK2 meter (manufactured by Geonics Limited, Mississauga, Ontario) was used in this study.<sup>1</sup> In either dipole orientation, this EMI meter provides simultaneous measurements of both the quadrature (apparent conductivity,  $EC_a$ ) and the in-phase (apparent magnetic susceptibility, IP) components. Apparent conductivity is expressed in milliSiemens/meter (mS/m). The IP response is expressed in parts per thousand (ppt) of the primary magnetic field generated by the transmitter. In this study,  $EC_a$  data were not corrected to a standard temperature of 75° F, and the IP data were not corrected for drift.

Operating procedures for the EM38-MK2 meter are described by Geonics Limited (2009). The EM38-MK2 meter operates at a frequency of 14.5 kHz and weighs about 11.9 lbs. The meter has one transmitter coil and two receiver coils, which are separated from the transmitter coil at distances of 1.0 and 0.5 m. This configuration provides two nominal exploration depths of 1.5 and 0.75 m when the meter is held in the vertical dipole orientation (VDO), and 0.75 and 0.40 m when the meter is held in the horizontal dipole orientation (HDO). However, these nominal depths of exploration are more restricted for IP measurements (Geonics Limited, 2009). When operated in the VDO and the in-phase mode, Dalan

---

<sup>1</sup> Manufacturer's names are provided for specific information; use does not constitute endorsement.

(2006) and Tabbagh (2009) reported that the EM38 meter has an effective penetration depth of only 40 to 50 cm.

An Allegro CX field computer (manufactured by Juniper Systems, Logan, Utah) and a Trimble AgGPS 114 L-band DGPS (differential global positioning system) receiver (manufactured by Trimble Navigation, Sunnyvale, CA) were used with the EM38-MK2 meter.<sup>2</sup> With these components, the EM38-MK2 meter is keypad operated and measurements are automatically triggered. The RTmap38MK2 software program developed by Geomar Software Inc. (Mississauga, Ontario) was used with the EM38-MK2 meter and the Allegro CX field computer, to record, store, and process EMI and GPS data.<sup>2</sup>

To help summarize the results of the EMI surveys, SURFER for Windows (version 10.0), developed by Golden Software, Inc. (Golden, CO), was used to construct the simulations shown in this report.<sup>2</sup> Grids of EMI data were produced using kriging methods with an octant search.

An Innov-X, Delta Standard portable X-ray fluorescence (P-XRF) spectrometer (manufactured by Olympus of Woburn, MA) was used by the New Jersey NRCS Soil Staff to assess the concentration of different metals in the soil samples collected at the Curtis Churchill Farm.<sup>2</sup> Samples were scanned with the P-XRF operated in a bench-top mode.

### Study Sites:

Study sites are located in cultivated fields that are principally mapped as phases of Lenzburg soils. The Lenzburg series is a member of the fine-loamy, mixed, active, calcareous, mesic Haplic Udarents taxonomic family. The very deep, well drained Lenzburg soils formed in excavated materials from surface coal-mining operations. The Lenzburg regolith is calcareous, loamy till that contains a mixture of loess and residuum from excavated siltstone, sandstone, shale, and limestone. By law, the Lenzburg soil must be a minimum of 48 inches thick, including topsoil and subsoil. Some areas may contain refuse materials from coal processing, locally known as gob or slurry. Gob and slurry are, respectively, coarse and fine waste from the coal cleaning processes. These materials can be acid-forming and toxic to plants.

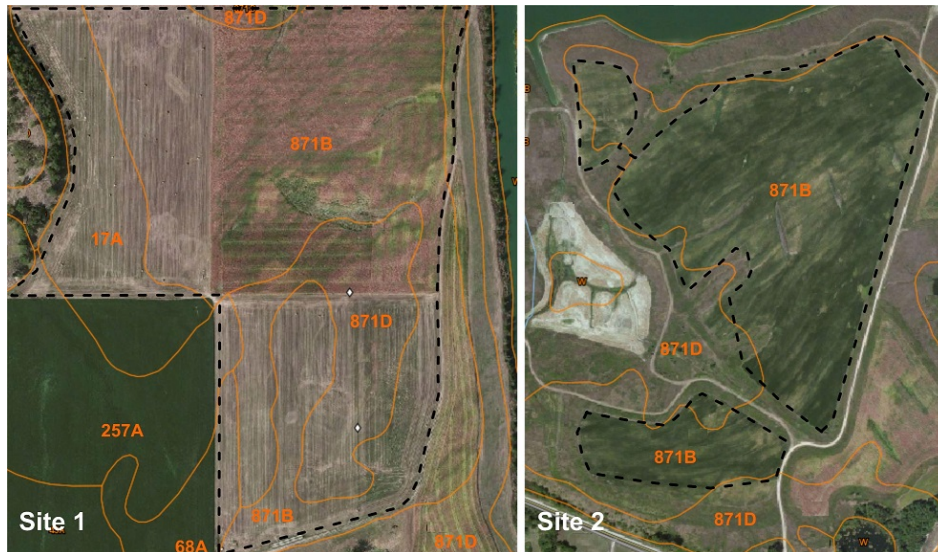


Figure 2. These soil maps of the study sites in Fulton County are from the Web Soil Survey. Soil samples were collected from the fields shown on the left for X-ray fluorescence analysis.

<sup>2</sup> Manufacturer's names are provided for specific information; use does not constitute endorsement.

Figure 2 contains soil maps of the two study sites from the Web Soil Survey.<sup>3</sup> Study Site 1 consists of three fields on the farm of Curtis Churchill, which is located about 1.0 kilometer east-northeast of Cuba, Illinois. These fields were mined in 1954 and 1955 with a shovel and bucket-wheel excavator combination and later graded (Spindler, 1981). Though principally mapped as different phases of Lenzburg soils (871B & 871D), two of these fields contain small areas of Keomah (fine, smectitic, mesic Aeric Endoaqualfs), Sable (fine-silty, mixed, superactive, mesic Typic Endoaquolls), and Clarksburg (fine-loamy, mixed, superactive, mesic Oxyaquic Fragiudalfs) soils. The very deep, somewhat poorly drained Keomah and poorly drained Sable soils formed in loess on moraines and stream terraces. The very deep, moderately well drained Clarksburg soils formed in colluvium, glacial till, or residuum weathered from limestone, shale, and sandstone on uplands.

Study site 2 is located on DoubleCluck Farm about 4.1 km northwest of Canton, Illinois. Two different slope phases (871B & 871D) of Lenzburg soils are mapped at this study site. Table 1 list the soil map units identified at these study sites.

**Table 1. Soil Map Units Delineated at the Study Sites in Fulton County**

Symbol	Map Unit Name
17A	Keomah silt loam, 0 to 2 % slopes
68A	Sable silty clay loam, 0 to 2 % slopes
257A	Clarksburg silt loam, 0 to 2 % slopes
871B	Lenzburg silt loam, 1 to 7 % slopes
871D	Lenzburg silt clay loam, 7 to 20 % slopes

**Survey procedures:**

The EM38-MK2 meter was pulled behind a Polaris Ranger utility vehicle on a *jet sled* at speeds of about 3 to 5 m/hr. The meter was operated in the deeper-sensing VDO with its long axis orientated parallel with the direction of travel. Data were recorded at a rate of two measurements per second.

At the Churchill Farm site, a minimum number of soil sampling points were selected by submitting the IP data to the *Response Surface Sampling Design* (RSSD) program of the ESAP (*EC<sub>e</sub> Sampling, Assessment, and Prediction*) software (Lesch, 2005; Lesch et al., 2000). The RSSD program was used to statistically select a small number of sample locations based on the observed magnitudes and spatial distribution of the IP data. Based on IP measurements, 12 optimal sampling points were identified in both the northwestern field and the eastern two fields. Small grab samples were collected from the 0 to 30 cm and 30 to 60 cm depth intervals at each of these sampling points. At the time of sampling, additional IP measurements were recorded over each sampling point. Measurements were not compensated for instrument drift.

At the New Jersey State NRCS office, the samples were dried and analyzed in sampling bags positioned at a constant distance from the P-XRF, which was mounted on a portable workstation. The spectrometer was calibrated by collecting a spectrum on a known standard (Alloy 316 stainless steel), and comparing the resulting values with the factory calibration standards. Each sample was scanned for 60 seconds. For each sample, scans were repeated two times and an average value was calculated. The P-XRF determined the contents of 15 elements (K, Ca, Ti, Cr, Mn, Fe, Co, Cu, Zn, As, Rb, Sr, Zn, Ba, and Pb). However, because of their very low concentrations, values for Cu, Zn, As and Pb were not recorded. On the P-XRF

<sup>3</sup> Soil Survey Staff, Natural Resources Conservation Service, United States Department of Agriculture. Web Soil Survey. Available online at <http://websoilsurvey.nrcs.usda.gov/>. Accessed [05/06/2014].

display, concentrations are expressed in parts per million, but are commonly communicated in milligrams per kilogram.

**Results:**

*Churchill Farm:*

Table 2 lists basic statistics for the EMI data collected with the EM38-MK2 meter at the Churchill Farm. In this and all subsequent tables of EM38-MK2 data, EC<sub>a</sub> recorded at nominal penetration depths of 0 to 150 and 0 to 75 cm are listed as 100EC<sub>a</sub> and 50 EC<sub>a</sub>, respectively. Also, in-phase measurements recorded with intercoil spacings of 100 and 50 cm are listed in the tables as IP100 and IP50, respectively.

**Table 2. Basic EMI statistics for the Churchill Farm Study Site (April 2014).**  
With the exception of “Number”, EC<sub>a</sub> values are in mS/m and IP values are in ppt.

	100EC <sub>a</sub>	50EC <sub>a</sub>	100IP	50IP
<b>Number</b>	14392	14392	14392	14392
<b>Minimum</b>	13.2	-79.5	-10.3	-17.2
<b>25%-tile</b>	39.0	33.3	-4.4	7.5
<b>75%-tile</b>	46.7	40.3	-2.2	15.8
<b>Maximum</b>	61.6	52.6	107.4	105.5
<b>Mean</b>	42.9	36.7	-3.1	12.5
<b>Std. Dev.</b>	5.2	5.2	2.7	7.1

Across the three survey fields, EC<sub>a</sub> mostly increased with increasing depth (measurements obtained with the deeper sensing 100EC<sub>a</sub> intercoil spacings were higher than those obtained with the shallower-sensing 50EC<sub>a</sub> intercoil spacings). This relationship is principally attributed to increasing soil moisture at deeper depths. For nominal exploration depths of 0 to 75 and 0 to 150 cm, EC<sub>a</sub> averaged 37 and 43 mS/m, respectively. For measurements recorded in the shallower-sensing (50EC<sub>a</sub>) intercoil spacing, one half of the EC<sub>a</sub> measurements were between 33 and 40 mS/m. For measurements recorded in the deeper-sensing (100EC<sub>a</sub>) intercoil spacings, one half of the EC<sub>a</sub> measurements were between 39 and 47 mS/m.

Across the three surveyed fields, the average IP response decreased with increasing intercoil spacing. The IP measurements were noticeably higher and more variable for the 50IP than the 100IP measurements (average values of 12 versus -3 ppt). The higher IP response in surface layers is attributed to differences in organic residue, surface moisture, soil compaction, and minerals (due to differences in fertilization, sludge applications, and management).

**Table 3. Basic EMI statistics for the Churchill Farm Study Site (April 2013).**  
With the exception of “Number”, EC<sub>a</sub> values are in mS/m and IP values are in ppt.

	100EC <sub>a</sub>	50EC <sub>a</sub>	100IP	50IP
<b>Number</b>	10580	10580	10580	10580
<b>Minimum</b>	25.0	-12.2	5.1	10.8
<b>25%-tile</b>	38.6	27.3	10.9	39.9
<b>75%-tile</b>	45.7	33.1	15.9	56.5
<b>Maximum</b>	63.1	45.9	87.7	94.5
<b>Mean</b>	42.3	30.3	13.5	48.7
<b>Std. Dev.</b>	4.8	4.2	3.6	10.3

Table 3 lists the basic statistics for measurements made with the EM38-MK2 meter across the three fields in April 2013. As data were recorded during the same month of the year and under presumably similar soil moisture and temperature conditions, values expressed in Tables 2 and 3 should be similar. While the

average  $EC_a$  values record during the two surveys are similar, average IP values were noticeably higher in April 2013. No explanation for the difference in IP values is possible at this time.

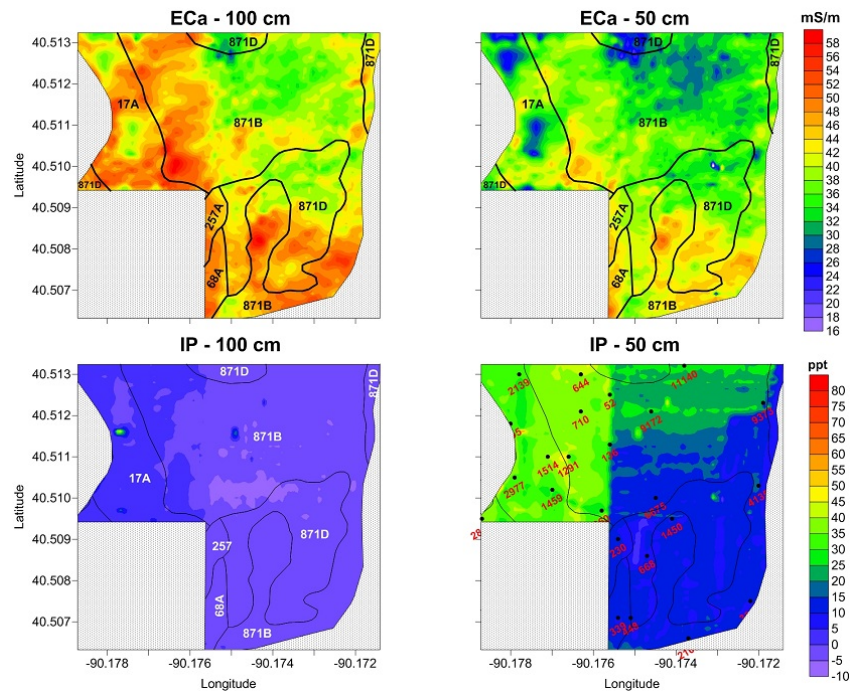


Figure 3. These plots of spatial  $EC_a$  and IP response patterns were obtained at the Churchill Farm in April 2014. Soil lines are from the Web Soil Survey. The locations of sample sites have been identified in the lower right plot.

Figure 3 contains plots of EMI data collected at the Churchill Farm with the EM38-MK2 meter in the shallower sensing 50-cm (right-hand plots) and deeper sensing 100-cm (left-hand plots) intercoil spacings. The upper and lower plots show spatial  $EC_a$  and IP patterns, respectively. To facilitate comparison, the same color scale and color ramp have been used for each data set ( $EC_a$  and IP). Soil samples were collected from the 0 to 30 cm and 30 to 60 cm depth intervals at twenty-four locations for analysis with P-XRF (analysis was completed by Edwin Muniz, Assistant State Soil Scientist, USDA-NRCS, Somerset, New Jersey). The location and identity of each of these sampling points are shown in the lower right-hand plot in Figure 3. The soil boundary lines shown in these plots were imported from the Web Soil Survey.

As evident in Figure 3,  $EC_a$  is lowest in the northeast field (upper right). The lower  $EC_a$  in this field is associated with its slightly higher relief, and differences in management and mining operations. On all plots shown in Figure 3, a noticeable change in EMI response is evident along the north-south boundary that separates the two northern fields. Apparent conductivity and IP responses are higher in the northwestern field than in the northeastern field. In general,  $EC_a$  is higher in the western and southern portions of the study site.

The spatial IP patterns shown in Figure 3 vary among the three fields and are therefore presumed to reflect differences in management. In addition, the relative magnitude of the IP response varies among the three fields. The northwestern field received municipal sludge about 4 to 6 years ago. This field and the northern part of the northeastern field have the highest IP response for measurements obtained with the 50-cm intercoil spacing. The southeastern field and the southern part of the northeastern field have lower IP responses. The magnitude of the IP-response varies with depth with higher and more variable

values recorded in the IP-50 cm than the IP-100 cm response. Compared with the subsoil, surface layers often have greater magnetic susceptibility due to higher organic contents (Bevan, 1994). Each of the three fields is under different rotations and therefore, organic residue, surface moisture, soil compaction, and minerals (due to differences in fertilization and management) can be expected to differ.

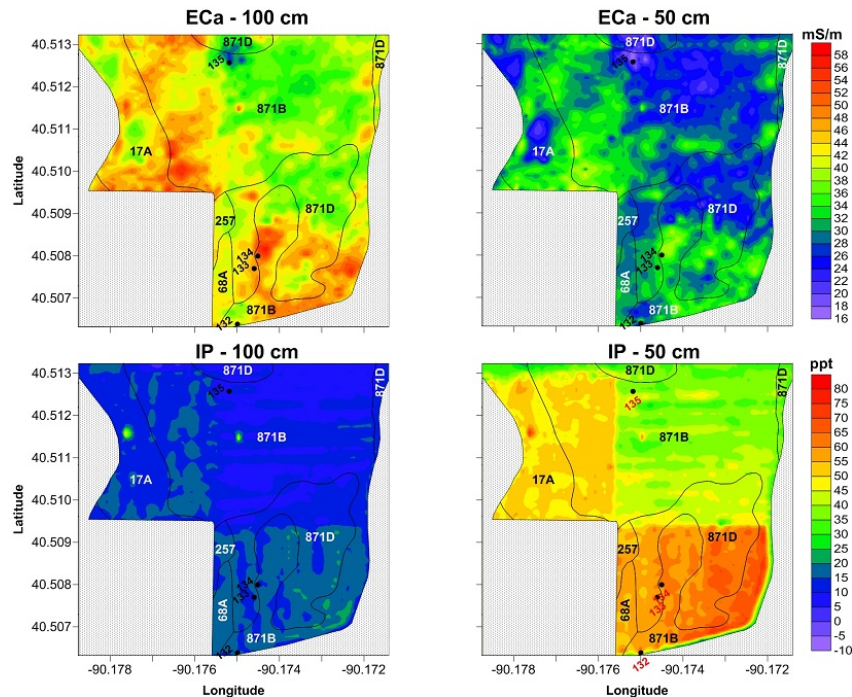


Figure 4. These plots of spatial  $EC_a$  and IP response patterns were obtained at the Churchill Farm in April 2013. Soil lines are from the Web Soil Survey. The locations of four sample sites have been identified in each plot.

Figure 4 contains plots of the EMI data that were collected at the Churchill Farm with the EM38-MK2 in April 2013. To facilitate comparison of the plots in this figure with those in Figure 3, the same color scales and color ramps have been used. The spatial  $EC_a$  patterns evident in these two figures are complex, but remarkable similar. Differences in  $EC_a$  values can be attributed to temporal variations in soil moisture contents and soil temperatures at the time of the two surveys. The IP response is noticeable higher and more variable at the time of the April 2013 survey (Figure 4) than April 2014 survey (Figure 3). For both surveys, the IP response measured with the 50-cm intercoil spacing is higher and more variable than the IP response measured with the 100-cm intercoil spacing. In the April 2013 survey, each of the three fields had noticeably different IP responses. However, in the April 2014 survey, only the northwestern field (the field that received municipal sludge) and the northern portion of the northeastern field appear to have anomalously high IP responses. As the IP responses were different among the fields, these differences were attributed to differences in field management. These differences in IP response and the known application of municipal sludge to the northwestern field prompt the use of X-ray fluorescence to measure the concentration of metals in these fields.

### P-XRF:

Portable X-ray fluorescence spectrometers use high energy (incident X-ray photon) to forcibly eject electrons from the inner shell of atoms. The resulting electron holes cause instability that result in outer shell electrons being dropped into the inner shell to fill the voids. This process results in the emission of energy, which is referred to as X-ray fluorescence. The energy emitted as fluorescence is element

specific, hence allowing the identification and quantification of different metals (Weindorf et al., 2012). A comprehensive discussion of P-XRF is provided by Kalnicky and Singhvi (2001).

At the Churchill Farm, soil samples were collected from the 0 to 30 and 30 to 60 cm depth intervals at 24 sampling points (see lower, right-hand plot in Figure 3 for the locations of these sites) for analysis with a P-XRF spectrometer. The twelve most abundant metals measured in these samples are listed in Table 4 and 5, which are for the 0 to 30 and the 30 to 60 cm depth intervals, respectively. This data documents the concentrations of twelve different metals across the three fields that were surveyed on the Churchill Farm and in areas of Lenzburg soils. These metals are (in order of abundance): Fe, K, Ca, Ti, Mn, Zr, Ba, Co, Sr, Rb, Cr, and Zn. In Tables 4 and 5, it can be seen that the concentrations of these metals varied over several orders of magnitude.

**Table 4. Concentration of metals in soil samples collected from the 0 to 30 cm depth interval.**

Data is expressed in parts per million (mg/kg).

OBS	K	Ca	Ti	Cr	Mn	Fe	Co	Zi	Rb	Sr	Zr	Ba
52	13137	13585	3330	47	489	23684	182	57	75	106	437	255
136	14599	13014	3699	53	600	29864	215	57	79	126	431	299
230	8286	5041	2551	46	311	19290	190	47	65	95	391	219
339	8576	8740	2735	48	229	18994	147	48	63	100	427	223
360	10425	6291	3051	58	665	25047	188	50	74	108	463	256
448	6298	8505	2119	40	208	16208	157	44	60	97	389	192
644	17901	7609	4355	72	476	32772	228	82	104	136	395	362
668	11739	11918	3221	38	296	21480	182	44	67	104	424	247
710	11259	5332	3089	57	512	20200	182	54	72	134	471	290
1291	8344	13555	2552	53	376	24300	265	71	75	112	341	227
1450	12553	12123	3203	44	445	23044	201	43	67	100	388	266
1459	11690	2982	3215	38	431	16271	166	45	75	106	535	243
1514	8427	2754	2786	40	464	14009	160	46	85	111	514	238
2106	10633	16042	2635	41	195	15543	161	43	60	108	408	237
2139	14112	5196	3956	62	665	25689	210	57	86	110	432	308
2495	13447	5711	3363	54	546	22642	255	57	78	112	466	292
2826	12541	15560	3120	47	464	20942	155	48	68	103	380	214
2977	12907	4664	3324	48	712	22523	207	59	77	106	477	311
3328	13205	10108	3392	51	348	24068	202	49	72	101	390	258
4135	13917	10518	3558	53	382	22610	183	49	72	111	445	326
6675	9956	7841	2564	40	366	22341	243	43	67	97	406	241
9172	13514	9029	3682	53	408	25636	243	49	75	101	439	251
9373	7032	4442	2502	55	500	23268	261	43	71	92	401	185
11140	8721	5504	2684	49	393	22433	263	55	72	101	398	231
<b>AVG:</b>	<b>11384</b>	<b>8586</b>	<b>3112</b>	<b>49</b>	<b>437</b>	<b>22202</b>	<b>202</b>	<b>51</b>	<b>73</b>	<b>107</b>	<b>427</b>	<b>257</b>

For both depth intervals, Fe was the most abundant element. The average concentration of Fe remained essentially constant at both soil depths. The average concentration of Fe for the 0 to 30 and the 30 to 60 cm depth intervals were 22,202 and 22,888 mg/kg, respectively. Potassium was the second most abundant element. The concentration of K also remained essentially constant with increasing soil depth. The average concentration of K for the 0 to 30 and the 30 to 60 cm depth intervals were 11,384 and 11,805 mg/kg, respectively. Calcium was the third most abundant metal. The concentration of Ca increased slightly (about 12%) with increasing soil depth (8,586 to 9,649 mg/kg for the 0 to 30 and the 30 to 60 cm depth intervals, respectively). Titanium was the fourth most abundant element. The

concentration of Ti remained essentially constant with increasing soil depth (3,112 and 3,256 mg/kg for the 0 to 30 and the 30 to 60 cm depth intervals, respectively). Manganese was the fifth most abundant metal. The concentration of Mn increased slightly (about 15%) with increasing soil depth (from 437 and 501 mg/kg for the 0 to 30 and the 30 to 60 cm depth intervals, respectively).

**Table 5. Concentration of metals in soil samples collected from the 30 to 60 cm depth interval.**

Data is expressed in parts per million (mg/kg).

OBS	K	Ca	Ti	Cr	Mn	Fe	Co	Zi	Rb	Sr	Zr	Ba
52	14279	14832	3722	69	719	23886	229	50	76	120	493	292
136	12208	11773	3181	56	436	27187	220	67	82	114	377	311
230	7483	7762	2422	48	335	20702	199	47	67	99	410	230
339	12762	16247	3371	55	251	20534	223	47	70	111	462	280
360	14262	10413	3779	65	709	24581	230	47	77	123	483	305
448	9042	16700	2633	45	232	19213	207	45	65	108	425	229
644	15059	9280	3871	60	603	28831	229	57	86	110	388	322
668	12259	22093	3105	54	322	22637	192	45	66	107	362	210
710	12909	7854	3698	67	839	32133	190	71	75	102	423	294
1291	13275	10676	3888	58	527	27102	201	46	72	106	463	270
1450	8916	8079	2761	49	346	23222	217	44	70	92	371	232
1459	13900	3676	3681	58	568	26593	265	65	81	107	521	360
1514	12041	3463	3408	46	659	18619	187	54	98	106	470	319
2106	11207	8917	2955	48	171	15284	161	46	69	119	430	256
2139	13445	3734	3716	57	679	22163	177	55	82	104	507	330
2495	5185	1914	1860	40	282	11340	143	39	74	86	413	188
2826	13487	12038	3418	47	628	20203	190	48	74	113	446	278
2977	13028	4939	3519	58	610	26344	263	58	75	105	485	303
3328	13593	16485	3375	58	519	24881	173	46	66	119	435	277
4135	14103	14052	3474	43	531	23491	207	53	75	116	471	294
6675	12478	5024	3489	49	600	28411	242	46	76	104	428	299
9172	8128	5232	2835	60	451	24716	207	52	76	102	430	237
9373	8447	2802	2845	52	513	16121	207	50	75	94	485	241
11140	11841	13602	3140	45	490	21114	196	52	70	102	419	250
<b>AVG:</b>	<b>11805</b>	<b>9649</b>	<b>3256</b>	<b>53</b>	<b>501</b>	<b>22888</b>	<b>206</b>	<b>51</b>	<b>75</b>	<b>107</b>	<b>441</b>	<b>275</b>

Table 6 lists the correlations between the IP and the P-XRF data for all samples collected at the Churchill Farm (24 samples from both the 0 to 30 and the 30 to 60 cm depth intervals). Because of the small number of samples collected, non-parametric statistics were used to evaluate the associations among the measured heavy metals and the IP responses. For both depth intervals correlations were mostly low and non-significant. However, for the 0 to 30 cm depth interval, moderate, negative, and significant ( $p = 0.01$ ) correlations were obtained between IP100 and Mn ( $r = -0.53$ ) content. Also, for the 30- to 60-cm depth interval, moderate, negative, and significant ( $p = 0.01$ ) correlations were obtained between IP50 response and the concentration of Mn ( $-0.55$ ) and Ru ( $r = -0.56$ ) contents. A moderate, negative, and significant ( $p = 0.01$ ) correlation was also obtained between the IP100 response and the concentration of Mn ( $-0.59$ ). No satisfactory explanation can be made at this point in the study for these relationships.

The study area at the Churchill Farm is partitioned into fields 1 (southeastern-most), 2 (northeastern-most), and 3 (northwestern-most). As a result of the spatial IP patterns evident in Figure 3 and knowledge of the sludge applications to field 3, the fields were grouped into two areas: fields 1 & 2 (combined), and field 3. The average concentrations of the selected metals in each of the two areas were

compared and this data is shown in Table 7. With the exception of Ca and Co, the concentrations of all other analyzed metals are higher in field 3 than in fields 1 & 2. This may be related to the known application of sludge on field 3. Notably, for soil sampled from the 0 to 60 cm depth, the concentration of Mn is 55 % higher in field 3 than in fields 1 & 2. Conversely, for soil sampled from the 0 to 60 cm depth, the concentration of Ca was 18 % higher in field 1 & 2 than in field 3. However, the concentration of K and Zi are 19 %, higher in field 3 than in fields 1 & 2.

**Table 6. Spearman’s rank correlation coefficients for IP responses and element concentrations for all samples collected at the Churchill Farm.**

0-30 cm	K	Ca	Ti	Cr	Mn	Fe	Co	Zi	Ru	Sr	Zr	Ba
IP50	-0.34	-0.13	-0.41	-0.30	-0.38	-0.40	-0.27	-0.39	-0.51	-0.40	-0.19	-0.25
IP100	-0.42	0.040	-0.47	-0.39	-0.53*	-0.49	-0.50	-0.33	-0.49	-0.35	-0.15	-0.28
30-60 cm	K	Ca	Ti	Cr	Mn	Fe	Co	Zi	Ru	Sr	Zr	Ba
IP50	-0.42	0.08	-0.53	-0.42	-0.55*	-0.30	-0.12	-0.26	-0.56*	-0.14	-0.26	-0.39
IP100	-0.16	0.38	-0.29	-0.31	-0.59*	-0.34	0.029	-0.39	-0.47	0.07	-0.13	-0.28

\* Indicates significance at the .01 level.

**Table 7. Differences in the average concentration of selected metals between Field 3 and Fields 1 for two soil depth intervals at the Churchill Farm.**

Data is expressed in parts per million (mg/kg).

Depth	Location	K	Ca	Ti	Cr	Mn	Fe	Co	Zi	Ru	Sr	Zr	Ba
0-30	Field 3	12399	8021	3320	52	533	23162	201	57	79	114	445	274
	Fields 1&2	10369	9151	2904	46	340	21243	203	46	68	100	409	239
	Difference	2030	-1130	416	6	193	1919	-2	10	11	14	36	35
30-60	Field 3	12756	7882	3478	56	605	24082	210	54	79	108	456	298
	Fields 1&2	10855	11416	3034	50	397	21693	202	48	70	106	427	253
	Difference	1902	-3534	445	6	208	2388	8	7	9	2	29	45

The next step was to explore if any relationship exists between IP response and the concentration of metals within these two areas (Fields 1 & 2, and field 3). The derived Spearman rank correlation coefficients are shown in tables 8 and 9.

**Table 8. Spearman’s rank correlation coefficients for IP responses and element concentrations for all samples collected in fields 1 & 2 at the Churchill Farm.**

0-30 cm	K	Ca	Ti	Cr	Mn	Fe	Co	Zi	Ru	Sr	Zr	Ba
IP50	-0.39	-0.03	-0.49	-0.32	-0.47	-0.64**	-0.47	-0.10	-0.60*	-0.21	-0.62**	-0.30
IP100	-0.43	0.26	-0.50	-0.47	-0.63**	-0.80**	-0.77**	-0.23	-0.80**	0.03	-0.41	-0.24
30-60 cm	K	Ca	Ti	Cr	Mn	Fe	Co	Zi	Ru	Sr	Zr	Ba
IP50	-0.35	0.07	-0.60	-0.35	-0.54*	-0.38	-0.34	-0.45	-0.68**	0.04	-0.24	-0.29
IP100	-0.05	0.44	-0.31	-0.44	-0.78**	-0.50	-0.15	-0.58*	-0.70**	0.15	-0.20	-0.22

\*and \*\* Indicates significance at the .05 and .01 levels.

Surprisingly, the correlations between IP response and the concentration of metals were generally higher in Fields 1 & 2 (Table 8) than in Field 3 (Table 9). In Fields 1 & 2, for the 0 to 30 cm depth interval, moderate to high correlations were obtained between IP responses and Fe and Ru concentrations. A moderate correlation was also obtained between the IP50 response and the concentration of Zr. In addition, for the 0 to 30 cm depth interval, moderate to high correlations were also obtained between the IP100 response and the concentration of Mn and Co. For the 30 to 60 cm depth interval, moderate to high correlations were obtained between IP responses and Zi, Mn and Ru concentrations.

In Field 3, correlations between IP response and the concentrations of different metals were low and non-significant. However, for the 0 to 30 cm depth interval, a moderate correlation was obtained between IP50 responses and the concentration of Mn and the IP100 response and the concentration of Ca.

**Table 9. Spearman’s rank correlation coefficients for IP responses and element concentrations for all samples collected in field 3 at the Churchill Farm.**

0-30 cm	K	Ca	Ti	Cr	Mn	Fe	Co	Zi	Ru	Sr	Zr	Ba
IP50	0.12	-0.51	0.09	-0.01	0.60*	-0.13	-0.10	-0.22	-0.12	-0.08	0.41	0.29
IP100	-0.09	-0.58*	-0.05	-0.14	0.24	-0.22	-0.16	-0.05	0.16	-0.31	0.52	0.10
30-60 cm	K	Ca	Ti	Cr	Mn	Fe	Co	Zi	Ru	Sr	Zr	Ba
IP50	-0.22	-0.51	-0.26	-0.23	-0.08	-0.05	0.19	0.16	-0.17	-0.30	0.02	-0.04
IP100	0.17	-0.29	0.17	0.22	0.18	-0.01	0.55	-0.14	0.14	0.15	0.52	0.23

\* Indicates significance at the .05 level.

*DoubleCluck Farm:*

In general, at the DoubleCluck Farm,  $EC_a$  increased and became slightly more variable with increasing depth. Table 10 lists the basic statistics for the EMI data collected at the DoubleCluck Farm. With the EM38-MK2 meter, for nominal exploration depths of 0 to 75 and 0 to 150 cm,  $EC_a$  averaged 28 and 42 mS/m, respectively. For measurements recorded with the shallower-sensing 50-cm intercoil spacing, one half of the recorded  $EC_a$  data were between 24 and 31 mS/m. For measurements recorded with the deeper-sensing 100-cm intercoil spacing, one half of the recorded  $EC_a$  data were between 39 and 46 mS/m.

At the DoubleCluck Farm study site, IP measurements were noticeably higher for the 50IP than for the 100IP measurements (average values of 20 versus 3 ppt, respectively). In addition, the range in IP measurements was noticeably different for the two intercoil spacings (about -7 to 201 ppt and -1 to 116 ppt recorded for the 50IP and the 100IP measurements, respectively). These differences are presumed to reflect differences in soil magnetic properties caused by differences in management and the possible occurrence of near-surface metallic objects scattered across the site.

**Table 10. Basic EMI statistics for Study Site 2 in Fulton County, Illinois.**

With the exception of “Number”,  $EC_a$  values are in mS/m and IP values are in ppt.

	100 $EC_a$	50 $EC_a$	100IP	50IP
<b>Number</b>	8653	8653	8653	8653
<b>Minimum</b>	10.2	11.9	-0.9	-7.3
<b>25%-tile</b>	38.9	24.4	1.8	18.1
<b>75%-tile</b>	45.6	30.8	3.7	21.2
<b>Maximum</b>	64.9	50.2	116.1	201.3
<b>Mean</b>	42.4	27.7	2.9	19.8
<b>Std. Dev.</b>	4.9	4.5	2.2	3.3

Figure 5 contains plots of the EMI data collected at DoubleCluck Farm with the EM38-MK2 meter for both the shallower-sensing 50-cm (left-hand plots) and deeper-sensing 100-cm (right-hand plots) intercoil spacings. The upper and lower plots show spatial  $EC_a$  and IP data, respectively. To facilitate comparison, the same color scale and color ramp have been used for each similar data set ( $EC_a$  and IP).

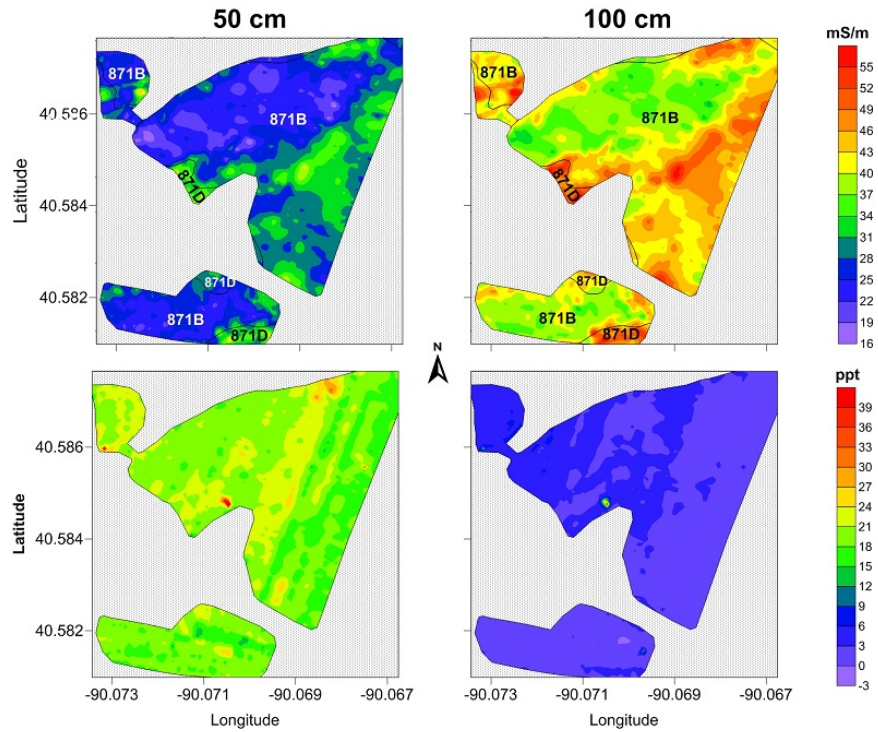


Figure 5. These plots of spatial  $EC_a$  and IP response patterns were obtained at Study Site 2 from data collected with an EM38-MK2 meter operated in the 100-cm (left-hand plots) and the 50-cm (right-hand plots) intercoil spacing. Soil lines are from the Web Soil Survey.

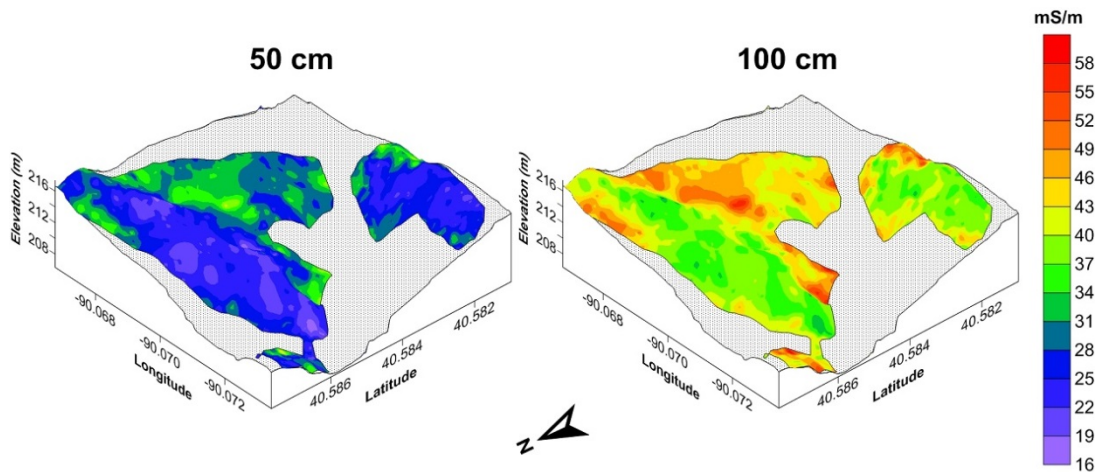


Figure 6. In these 3D simulations, alternating patterns of higher and lower  $EC_a$  appear to cross the Double Cluck farm study site in northeast to southwest trending strips

In the plots of the  $EC_a$  data shown in Figure 5, higher values are recorded in the eastern half of most fields. In addition, alternating, northeast to southwest trending strips of higher and lower  $EC_a$  are evident. These patterns are presumed to reflect surface mining operations and reclamation processes as they cut directly across the landscape and contours (see Figure 6). Compared with the spatial  $EC_a$  patterns, spatial IP patterns are more subdued. The spatial IP patterns shown in Figure 5 (lower plots) tend to follow the general directions in which the fields were surveyed [with EMI] and cultivated. Several anomalous

values can be seen in the two plots of IP data. These values are presumed to reflect the presence of metallic artifacts buried or scattered across these cultivated fields.

## Technical Report on Ground-Penetrating Radar (GPR) Investigations conducted in Jo Daviess County, Illinois on 1 May 2014.

This study was initiated after repeated observations on intersecting linear patterns of differing plant vigor and growth in areas of Frankville soils. These observations were made by the Illinois Geological Survey and NRCS soil scientists, conservationists, and agronomists. The vegetal pattern (Figure 7) is the result of intersecting joints or crack in the underlying limestone bedrock. These cracks impact water and gas movement through bedrock, and influence plant rooting depths and available soil moisture. These patterns are more evident in dry years and under conditions of plant-soil moisture stress. Because of their relative abundance and spatial extent, these joint patterns may need to be considered in the design and interpretations of several soil map units.



Figure 7. Differing patterns of alfalfa vigor and growth are evident in an area of Massbach silt loam, 2 to 5 percent slopes, in Jo Daviess County, Illinois.

### Study Site:

The study site is located in an alfalfa field (N 42° 26.986', W 89° 59.092) that is mapped as Massbach silt loam, 2 to 5 percent slopes (753B). The deep, moderately well drained Massbach soil formed in loess over residuum weathered from calcareous shale. However, soils at this site were identified as Frankville (Roger Windhorn, personal communication). The moderately deep, well drained Frankville (fine-silty, mixed, superactive, mesic Mollic Hapludalfs) soils formed in loess and residuum weathered from dolomitic limestone. Frankville soils are considered moderately suited to GPR.

### Equipment:

Ground-penetrating radar, or GPR, is a time-scaled system. This geophysical tool measures the time it takes for pulses of electromagnetic energy to travel from an antenna to a subsurface interface (boundary) and back. Whenever a transmitted pulse contacts an interface separating materials with different dielectric properties, a portion of the energy is reflected back to the receiving antenna. The more abrupt

and contrasting the dielectric properties on opposing sides of an interface, the greater the amount of energy that is reflected back to the antenna and the greater the amplitude of the recorded signal.

The radar unit used in this study is the TerraSIRch Subsurface Interface Radar (SIR) System-3000 (here after referred to as the SIR-3000), manufactured by Geophysical Survey Systems, Inc. (GSSI; Salem, NH).<sup>4</sup> The SIR-3000 consists of a digital control unit (DC-3000) with keypad, SVGA video screen, and connector panel. A 10.8-volt lithium-ion rechargeable battery powers the system. The SIR-3000 weighs about 4.1 kg and is backpack portable. With an antenna, the SIR-3000 requires two people to operate. Jol (2009) and Daniels (2004) discuss the use and operation of GPR. A relatively high frequency, 400 MHz antenna was used in this study. The 400 MHz antenna provided good resolution and suitable depths of exploration in this area of Frankville soils. A distance-calibrated survey wheel with encoder was bolted onto the antenna and provided control over signal pulse transmission and data collection along radar traverse lines (Figure 8).



Figure 8. Dan Withers (Cartographer, Champaign, IL) and Michael England (Soil Scientist, Onalaska, WI) conduct a bedrock survey with GPR.

The RADAN for Windows (version 7.0) software program (developed by GSSI) was used to process the radar records<sup>4</sup>. Processing methods used included: header editing, setting the initial pulse to time zero, color table and transformation selection, signal stacking, and horizontal high pass filtration (refer to Jol (2009) and Daniels (2004) for discussions of these techniques). In addition, range gain adjustments were used on radar records to improve pattern recognition.

#### **Calibration of GPR:**

Ground-penetrating radar is a time scaled system. To convert the travel time into a depth scale, either the velocity of pulse propagation or the depth to a reflector must be known. The relationships among depth (D), two-way pulse travel time (T), and velocity of propagation (v) are described in equation [1] (after Daniels, 2004):

---

<sup>4</sup> Manufacturer's names are provided for specific information; use does not constitute endorsement.

$$v = 2D/T \quad [1]$$

The velocity of propagation is principally affected by the relative dielectric permittivity ( $\epsilon_r$ ) of the profiled material(s) according to equation [2] (after Daniels, 2004):

$$\epsilon_r = (C/v)^2 \quad [2]$$

In equation [2],  $C$  is the velocity of light in a vacuum (0.984 ft/ns). In soils, the amount and physical state (temperature dependent) of water have the greatest effect on the  $\epsilon_r$  and  $v$ . Dielectric permittivity ranges from 1 for air, to 78 to 88 for water (Cassidy, 2009). Small increments in soil moisture can result in large increases in the relative permittivity of soils (Daniels, 2004).

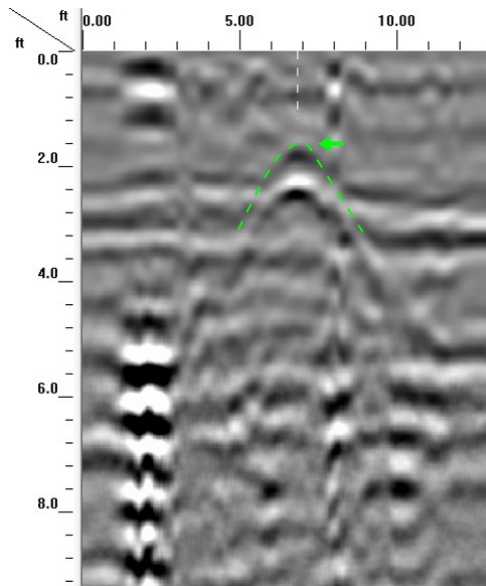


Figure 9. The arrow points to a reflection hyperbola from a metal plate, which was buried at depth of 20 inches. On this radar record, the reflection hyperbola has been highlighted with a segmented green line. All scales are in feet.

To adjust the depth scale, a GPR traverse was conducted across a metal plate that was buried at a depth of 20 inches. Figure 9 is the radar record from this traverse. In Figure 9, the horizontal (distance) and vertical (depth) scales are expressed in feet. The metal reflector has produced a high-amplitude reflection hyperbola. The hyperbola has a characteristic inverted V-shape (marked and highlighted with green arrow in Figure 9). Using this depth, the recorded two-way travel time to this feature (8.0 ns), and equation [1], the average velocity of signal propagation was estimated to be 0.4169 ft/ns. Using equation [2], the average  $\epsilon_r$  was estimated to be 5.6. This information was used to depth scale the radar records.

### Interpretations:

Figure 10 is a representative radar record from the Frankville grid site. On this radar record a green-colored, segmented line has been used to identify the inferred soil/bedrock interface. Along this traverse, the depth to bedrock averages 1.6 feet and ranges from 0.8 to 2.0 feet. While the approximate depth to the soil/bedrock interface can be reasonably accurately predicted, variations in its depth, topography, and the presence of a thin and discontinuous paleosol or layer of residuum overlying the rock surface, and rock fragments immediately overlying dolomitic limestone bedrock result in some ambiguity caused by variations in signal amplitudes, and superposed or partially masked signals.

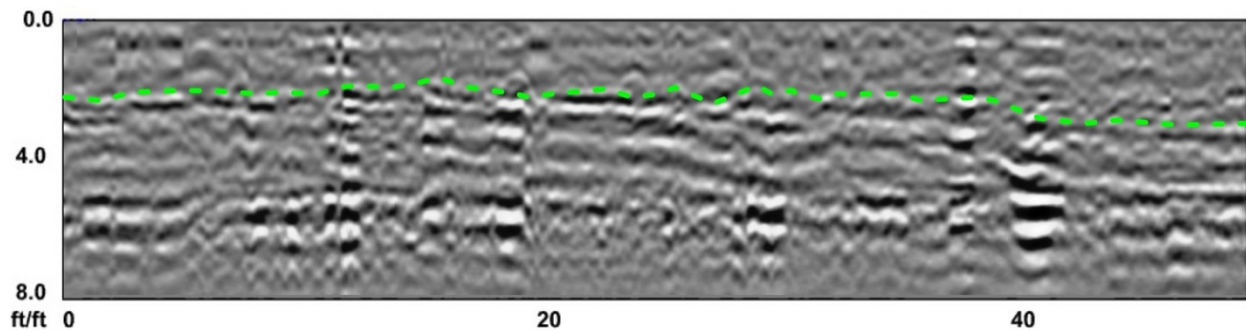


Figure 10. On this radar record from the grid site, the soil/bedrock interface is highlighted with a green, segmented line. All measurements are in feet.

### 3D Pseudo-Images and Amplitude Slice Analysis:

The effective visualization of collected radar data is the key to modern GPR interpretations. An emerging approach in GPR is the analysis of subsurface structures, distributions, and geometries from a three-dimensional (3D) perspective. This approach relies on programs and analysis techniques that were developed for processing seismic data. Three-dimensional GPR allows the rapid processing and visualization of data volumes from different perspectives and cross-sections (Beres et al., 1999). This can assist identification, outline the structure and geometry, and improve the interpretation of subsurface features. In areas of electrically resistive materials, Grasmueck and Green (1996) noted that, compared with two-dimensional (2D) GPR, 3D GPR can provide unrivaled resolution and detail of subsurface features. Beres et al. (1999) observed that 3D GPR improves the definition of subsurface structural trends and results in more complete and less ambiguous interpretations than traditional 2D GPR.

Three-dimensional GPR relies on the construction of a 3D pseudo-image of the subsurface within a gridded area. The gridded area is typically relatively small (between 3.3 to 26,900 ft<sup>2</sup>) and is intensively surveyed with multiple, closely-spaced (typically, 0.31 to 3.3 ft), parallel GPR traverse lines. This relatively dense network of grid lines is necessary to resolve the geometries and sizes of different subsurface features and to prevent spatially aliasing the data (Grasmueck and Green, 1996). Following data collection in the field, the radar data are processed into a 3D pseudo-image of the grid site. Once a 3D pseudo-image is constructed of a grid site, arbitrary cross-sections, insets, and time slices can be extracted from the data set. Interactive software packages enable the 3D pseudo image to be viewed from nearly any perspective (Junck and Jol, 2000). The RADAN 7.0 software program allows the users to animatedly travel through the entire data volume (Grasmueck, 1996).

One advanced signal processing method that is commonly used in 3D-GPR investigations is amplitude slice analysis (Conyers, 2004). This analysis technique explores differences in signal amplitudes within the 3D pseudo-image in "time-slices" (or depth-slices). In each time-sliced image, the reflected radar energy is averaged horizontally among adjacent, parallel radar traverses and in specified time (or depth) windows. Each time-sliced image displays changes in signal amplitudes within specific depth intervals of the soil (Conyers, 2004). Although the terms "time-slice" and "depth slice" are used interchangeably, only the term "depth-slice" will be used in this report.

### Survey Procedures:

A survey grid, with dimensions of 50 by 50 feet, was established across a relatively level area in the alfalfa field. The approximate coordinates and elevations of the grid corners are listed in Table 11. These

measurements were obtained with GPS. To facilitate the construction of the grid, two parallel lines were laid out and served as grid axis lines. Along these parallel axis lines, survey flags were inserted into the ground at a spacing of 2 ft. A rope was stretched between matching survey flags on these two axis lines, which were located on opposing sides of the grid area (50 ft apart), and the 400 MHz antenna was towed along the rope for guidance. Following data collection along the line, the rope was sequentially displaced 2 ft to the next pair of survey flags to repeat the process. Multiple GPR traverses were completed by pulling the 400 MHz antenna

**Table 11. Coordinates and elevations of the GPR Grid corners**

Latitude	Longitude	Elevation (m)
N 42° 26.986	W 89° 59.092	277
N 42° 26.993	W 89° 59.090	276
N 42° 26.993	W 89° 59.080	275
N 42° 26.986	W 89° 59.080	276

**Results:**

Surveys were completed of the grid site in both directions (along X- and Y-axis) in two separate surveys. However, combining the two grid sets did not improve interpretations over the data that were collected in only one direction. Background noise and a greater number of “signal artifacts” were evident and marred presentations that combined the data collected in two directions. Figure 11 is a 3D pseudo image of the grid site with the top 1.66 ft of soil material removed to reveal portions of the bedrock surface. In this pseudo-image all scales are in feet. The origin is located in the northwest corner of the grid site.

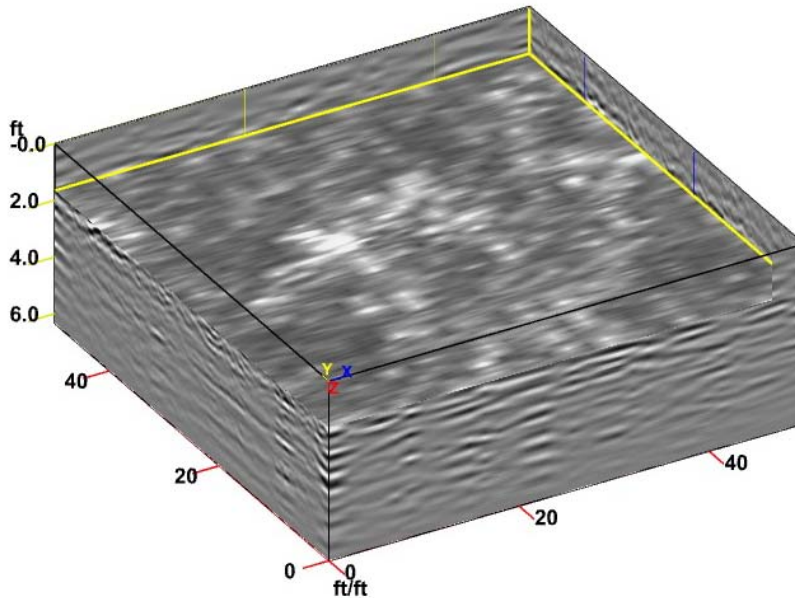


Figure 11. In this 3D pseudo-image of the grid site, the top 1.6 feet of the soil material has been removed to reveal portions of the bedrock surface, which appears as high-amplitude (colored white) reflections.

In the pseudo-image shown in Figure 11, a shallow area of bedrock is exposed in the central portion of the base of the removed inset cube. The bedrock surface produces high-amplitude reflections that appear as white-colored spatial pattern. On all sides of this shallower to bedrock area, the rock surface drops to slightly deeper depths and is not evident (areas appear darker colored) along the base of the inset cube. On the exposed sides of the pseudo-image, the layered structure of the bedrock can be observed.

Figure 12 contains four depth-sliced images of the grid area. These slices have been taken at approximate depths of 0, 1, 2, and 3 ft. In each image, the grid area (shown in Figure 11) is viewed from directly overhead. All dimensions are in feet. The origin of the grid ( $X = 0$  ft,  $Y = 0$  ft) is located in the northwest corner of the grid.

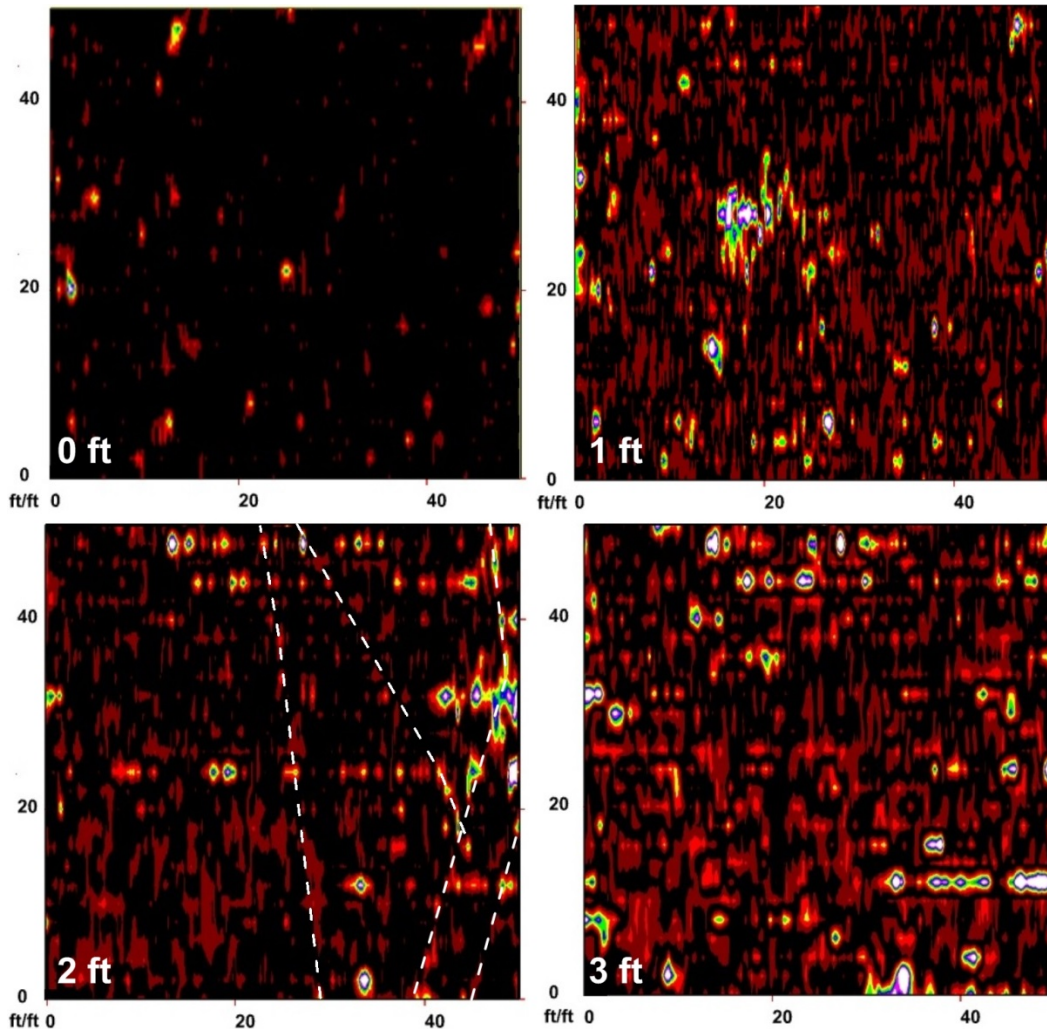


Figure 12. *These four horizontal depth-slice images from the Frankville grid site.*

On the depth-sliced images shown in Figure 12, variations in signal amplitude indicate spatial changes in soil properties. In the 0 ft depth-sliced image, areas shown in higher amplitudes (colored white, blue, yellow and red) probably represent chert or limestone fragments. Areas shown in black generally represented homogenous soil materials. In the 1 ft depth-sliced image, a greater number of high-amplitude reflections are apparent suggesting a greater number of rock fragments and perhaps a shallower area to bedrock (see clustering of high-amplitude reflections that are centered near  $X = 18$  ft,  $Y = 28$  ft). The 2 ft depth-sliced images is largely located within the top portion of the bedrock. The high-amplitude reflections that are aligned in a north-south orientation (left to right) parallel to the X axis represent system and signal processing noise. However, in this depth slice image, with a little stretch of the imagination, the alignment of several reflection patterns suggests several lineations, which have been highlighted with segmented white-colored lines. Though not marked, several linear reflection patterns can also be visualized in the 3 ft depth-sliced image.

Results from this investigation of joints in bedrock were disappointing. In a similar study that was conducted in an area of Farmington soils (loamy, mixed, active, mesic Lithic Eutrudepts) on the Tug Hill Plateau in northwestern New York, joint lineations were clearly evident on both 2D radar records and 3D pseudo-images (Doolittle et al., 2013). Looking at the soils of these two sites, one can note the dissimilarities between these two soils that results in differences in GPR performance. The average clay content of Farmington soils ranges from 10 to 27 percent, while that of Frankville soil is slightly higher with a range of 18 to 32 percent. Both soils are grouped into the mixed mineralogy class, but Farmington soil belongs to the active while Frankville soil belongs to the superactive cation-exchange activity class. Farmington soils are shallower to bedrock than Frankville soils with a range of 10 to 20 inches compared to about 20 to 40 inches. These differences will result in a greater rate of signal attenuation in Frankville than in Farmington soils. In addition, as already noted in this report, the observed area of Frankville soils has greater variations in the depth and topography of the bedrock surface than was observed at the Farmington site. In addition, for the Frankville soils, the presence of a thin and discontinuous paleosol or layer of residuum overlying the rock surface, and a greater concentration of rock fragments immediately overlying bedrock surface resulted in greater ambiguity of the soil/bedrock interface.

#### **References:**

- Beres, M, P. Huggenberger, A.G. Green, and H. Horstmeyer, 1999. Using two- and three-dimensional georadar methods to characterize glaciofluvial architecture. *Sedimentary Geology* 129: 1-24.
- Bevan, B., 1994. Remote sensing of gardens and fields. 70-90 pp. In: Miller, N. F., and K. L. Gleason (Eds.). *The Archaeology of Gardens and Fields*, University of Pennsylvania Press, Philadelphia, PA.
- Cassidy, N.J. 2009. Electrical and magnetic properties of rocks, soils, and fluids. In *Ground Penetrating Radar: Theory and Applications*, ed. H. M. Jol, 41-72 pp. Elsevier Science, Amsterdam, The Netherlands.
- Conyers, L.B., 2004. *Ground-Penetrating Radar for Archaeology*. Altamira Press, Walnut Creek, California (2004)
- Dalan, R., 2006. Magnetic Susceptibility. 162-203 pp. In: Johnson, J.K. (ed.), *Remote Sensing in Archaeology: An Explicitly North America Perspective*. Alabama Press, Tuscaloosa, Alabama.
- Daniels, D.J., 2004. *Ground Penetrating Radar; 2nd Edition*. The Institute of Electrical Engineers, London, United Kingdom.
- Doolittle, J.A., O. Vargas, A. Langer and R. Dobos, 2013. Crossing the Lines with GPR. *Soil Horizons* 54(4): 1-3. DOI: 10.2136/sh13-02-0010.
- Geonics Limited, 2009. EM38-MK2-2 ground conductivity meter operating manual. Geonics Ltd., Mississauga, Ontario.
- Grasmueck, M., 1996. 3-D ground-penetrating radar applied to fracture imaging in gneiss. *Geophysics* 61(4): 1050-1064.
- Grasmueck, M, and A.G. Green, 1996. 3-D georadar mapping: Looking into the subsurface. *Environmental and Engineering Geoscience Vol II (2)*: 195-220.
- Jol, H., 2009. *Ground Penetrating Radar: Theory and Applications*. Elsevier Science, Amsterdam, The Netherlands.

Junck, M.B., and H.M. Jol, 2000. Three-dimensional investigation of geomorphic environments using ground penetrating radar. 314-318 pp. In: Noon, D. (editor) Proceedings Eight International Conference on Ground-Penetrating Radar. May 23 to 26, 2000, Goldcoast, Queensland, Australia. The University of Queensland.

Kalnicky D.J., and R. Singhvi, 2001. Field portable XRF analysis of environmental samples. *Journal of Hazardous Materials* (83): 93-122.

Lesch, S.M. 2005. Sensor-directed response surface sampling designs for characterizing spatial variation in soil properties. *Computers and Electronic in Agriculture* 46: 153-180.

Lesch, S.M., J.D. Rhoades and D.L. Corwin. 2000. ESAP-95 version 2.10R User Manual and Tutorial Guide. Research Report 146. USDA-ARS George E. Brown, Jr. Salinity Laboratory, Riverside, California.

Spindler, D., 1981. Three case studies of row crop production on mined land. 493-495 pp. In *Proceedings of the Symposium on Surface Mining Hydrology, Sedimentology and Reclamation*. December 7-11, 1981, Lexington, Kentucky.

Tabbagh, A., 2009. Electromagnetic survey (EM38 Geonics LTD). 293-295 pp. In: Campana and Piro (eds.), *Seeing the Unseen - Geophysics and Landscape Archaeology*. Taylor & Francis Group, London.

Weindorf, D.C., Y. Zhu, B. Haggard, J. Lofton, S. Chakraborty, N. Bakr, W. Zhang, W.C. Weindorf, and M. Legoria. 2012. Enhance pedon horizonation using portable X-ray fluorescence spectrometry. *Soil Sci. Soc. Am. J.* 76:522–531. doi:10.2136/sssaj2011.0174